ChemComm

COMMUNICATION

View Article Online
View Journal | View Issue

Cite this: *Chem. Commun.*, 2023, 59, 13867

Received 1st September 2023,
Accepted 26th October 2023

DOI: 10.1039/d3cc04109c

rsc.li/chemcomm

Water vapour induced structural flexibility in a square lattice coordination network†

Kyriaki Koupepidou, Andrey A. Bezrukov, Dominic C. Castell, Debobroto Sensharma, Soumya Mukherjee and Michael J. Zaworotko *

Herein, we introduce a new square lattice topology coordination network, sql-(1,3-bib)(ndc)-Ni, with three types of connection and detail its gas and vapour induced phase transformations. Exposure to humidity resulted in an S-shaped isotherm profile, suggesting potential utility of such materials as desiccants.

Crystal engineering of coordination networks (CNs) has evolved from its initial focus upon design[1–3] into fine-tuning of structure/property relationships, thereby resulting in architectures that can be tailored to specific applications, especially gas storage and separation.[4–6] That CNs are typically amenable to design from first principles and can exhibit permanent porosity affords them with the potential to address topical environmental challenges, including direct air capture of CO_2,[7,8] separation of CO_2 from N_2 (*e.g.* flue gas remediation) or CH_4 (for natural gas refinement),[9,10] as well as atmospheric water harvesting (AWH).[11]

A feature of CNs that facilitates design is that they can be represented as topological blueprints that enable design of platforms of related CNs when deconstructed to nodes and linkers. For example, linear ditopic linker ligands and 4-connected metal nodes can yield platforms of **sql** (square lattice) or **dia** (diamondoid) topology CNs. In this context, linear pyridyl ditopic ligands (*e.g.* 4,4′-bipyridine) have been utilised to create platforms of **sql** networks of general formula ML_2X_2 (X = counteranion).[12–14] More recently, angular pyridyl ditopic ligands (*e.g.* 4,4′-dipyridylsulfide) have emerged as alternatives to their linear counterparts, sometimes offering ultramicropores that enable strong gas separation performance.[15–17] In these cases, such angular ligands can enable formation of spiro-linked 1D coordination polymers comprised of M_2L_2 loops (M = metal, L = ligand), which self-assemble with auxiliary dianionic linkers (L′) into 2D, typically **sql**, networks of general formula ML_2L'.

From a crystal engineering perspective, substitution of a pyridyl moiety with an imidazolyl in angular ligands should permit the same topological outcome. Herein, we focus on an imidazolyl angular linker ligand, 1,3-bib = 1,3-bis(imidazol-1-yl)benzene, which is understudied in the context of gas or vapour sorption.[18–20] Its linear analogue, 1,4-bib = 1,4-bis(imidazol-1-yl)benzene, was reported for its gas[21,22] or water vapour[23] sorption in flexible CNs. A survey on CNs sustained by 1,3-bib *vs.* 1,4-bib using the TOPOS TTO database[24] revealed that 1,3-bib forms mostly 2D networks with **sql** topology while 1,4-bib tends to afford 3D networks with **dia** or **pcu** (primitive cubic) topology (Fig. S1, ESI†). Analysis of the conformation of 1,3-bib and 1,4-bib in coordination compounds archived in the CSD (version 2023.2.0)[25] revealed that the two linkers are distinct from a crystal engineering point of view (Fig. S2–S5, ESI†). While 1,4-bib can sustain a narrow range of metal-to-metal (M–M) distances depending on if it is *syn* or *anti*, 1,3-bib allows more variety of M–M distances due to added complexity in the *syn* conformer, which can either be *endo* (leading to M_2L_2 loops) or *exo* (leading to tethering).

Water stable CNs offer potential for utility in AWH, for which a ''stepped'' or ''S-shaped'' water vapour isotherm profile is desirable as it offers increased working capacity and a low energy footprint compared to traditional desiccants with type I profiles.[26] This profile can be achieved either by rigid[27–29] or flexible[30–32] CNs, typically through pore-filling or gate-opening mechanisms, respectively. Even though flexible CNs offer potential for AWH,[33] water vapour induced structural flexibility in CNs remains understudied, with just 34 examples identified in a recent study (Table S1, ESI†),[34] despite the presence of >118 000 CNs in the cambridge structural database (CSD) database.[25] Furthermore, those CNs reported to undergo water vapour induced transformations are mostly 3D (Table S1, ESI†).

Motivated by the above, we exploited 1,3-bib to form a new 2D CN, $[Ni_2(1,3\text{-bib})_3(ndc)_2(H_2O)_2]_n$ or **sql-(1,3-bib)(ndc)-Ni** (ndc = 1,4-naphthalenedicarboxylate). Solvothermal reaction

Bernal Institute, Department of Chemical Sciences, University of Limerick, Limerick V94 T9PX, Republic of Ireland. E-mail: xtal@ul.ie

† Electronic supplementary information (ESI) available: Experimental details, PXRD patterns, TG traces, gas sorption isotherms, *etc*. CCDC 2288421–2288425. For ESI and crystallographic data in CIF or other electronic format see DOI: https://doi.org/10.1039/d3cc04109c

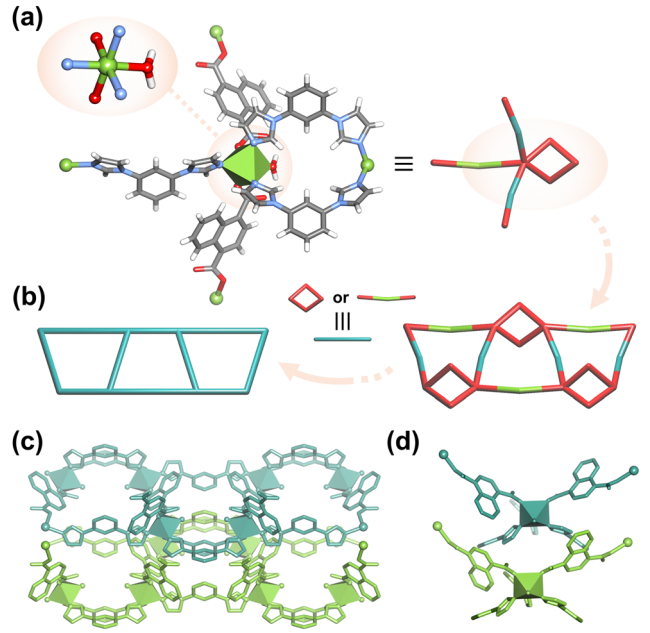

Fig. 1 (a) Coordination geometry around the Ni(II) centres; (b) [Ni_2(1,3-bib)$_2$] loop formation and topological analysis, simplified to **sql** net; (d) layered **sql** nets shown in cyan and green along the crystallographic *a* axis (c) and *c* axis (d). Hydrogen atoms are omitted for clarity in (c) and (d). Colour codes (for (a)): grey, C; red, O; blue, N; green, Ni.

of 1,3-bib, ndc and $Ni(NO_3)_2{\cdot}6H_2O$ afforded plate-shaped single crystals of **sql-(1,3-bib)(ndc)-Ni-α** (for experimental details see ESI†). Single-crystal X-ray diffraction (SCXRD) experiments revealed that **sql-(1,3-bib)(ndc)-Ni-α** had crystallized in the orthorhombic space group $Cmc2_1$ (Table S2, ESI†). The Ni(II) centres adopt octahedral coordination geometry, the two axial positions being occupied by an aqua ligand and a nitrogen atom from a 1,3-bib linker (Fig. 1a). The coordination sphere is completed by nitrogen atoms from different 1,3-bib linkers and oxygen atoms from two monodentate ndc linkers. Interestingly, there are three distinct types of connection: ndc linkers; a single 1,3-bib linker; a pair of 1,3-bib linkers that connect two adjacent Ni(II) centres, creating a [Ni_2(1,3-bib)$_2$] loop (Fig. 1b). Topologically, if this dimer is regarded as a two-point connection, the metal nodes can be simplified as 4-connected, classifying the structure as an **sql** net (see ESI† for detailed topological analysis). A CSD search (version 2023.2.0) revealed that, while this dimeric [M_2(1,3-bib)$_2$] moiety is common among 0D complexes sustained by 1,3-bib, it is present in only five other 2D CNs (Fig. S7 and Table S3, ESI†). Adjacent 2D nets in **sql-(1,3-bib)(ndc)-Ni-α** have inter-network Ni···Ni distances of 7.644 Å (Fig. 1c, d and Fig. S8, ESI†). Crystal packing of the 2D layers results in 1D channels accounting for a guest-accessible space of 16.2% of the unit cell volume (1018 Å^3, probe radius 1.2 Å). The channels are occupied by *N,N*-dimethylacetamide (DMA) and hydrate molecules, as confirmed by SCXRD (Fig. S9–S11, ESI†). Specifically, hydrate molecules occupy a special position between the two Ni centres, forming hydrogen bonds with the aqua ligands (O···O = 2.775 Å, Fig. S12, ESI†). Thermogravimetric (TG) analysis (Fig. S13, ESI†) showed that solvent loss was complete by 225 °C and Fourier transform infrared (FTIR) spectroscopy (Fig. S14, ESI†) was consistent with a hydrate. *In situ* variable temperature powder X-ray diffraction (VT-PXRD) measurements demonstrated that heating **sql-(1,3-bib)(ndc)-Ni-α** under N_2 flow did not trigger a phase change below 175 °C. Decomposition at 200 °C was accompanied by a change in colour from blue to green (Fig. S15 and S16, ESI†).

To activate without triggering decomposition, **sql-(1,3-bib)(ndc)-Ni-α** was exchanged with a more volatile solvent, methanol, resulting in a new phase, **sql-(1,3-bib)(ndc)-Ni-γ**, *via* a single-crystal to single-crystal (SC–SC) transformation (Fig. 2a and b). Although **sql-(1,3-bib)(ndc)-Ni-γ** had crystallised in the same space group as the parent compound and retained the same connectivity, a larger unit cell volume was observed, 6901.8 Å^3 *vs.* 6279.8 Å^3 (Table S2 and Fig. S17, ESI†). This unit cell expansion was accompanied by an increase in the guest-accessible space to 22.1% and enlargement of the interlayer distance to 8.550 Å (Fig. S8, ESI†). SCXRD data and a TG trace revealed that the hydrogen-bonded hydrate molecule between two Ni centres had remained, even though solvent molecules had been replaced by methanol (Fig. S18 and S19, ESI†). Differential scanning calorimetry (DSC) measurements suggested that another phase change occurred upon loss of methanol solvate molecules when heating **sql-(1,3-bib)(ndc)-Ni-γ** at *ca.* 60 °C. This is consistent with the endotherm observed at that temperature for the first heating cycle, but not for the second cycle (Fig. S20, ESI†). Indeed, heating **sql-(1,3-bib)(ndc)-Ni-γ** under vacuum induced transformation to a

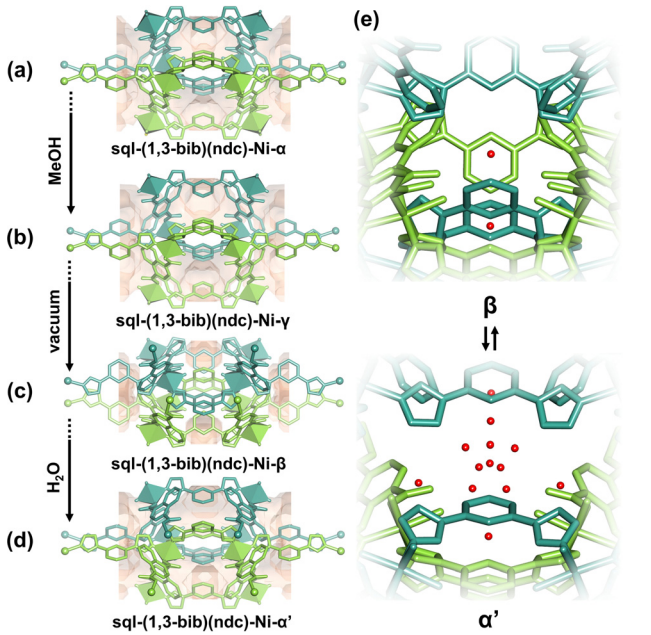

Fig. 2 Change in guest accessible space through structural transformations in **sql-(1,3-bib)(ndc)-Ni-α** (a), **sql-(1,3-bib)(ndc)-Ni-γ** (b), **sql-(1,3-bib)(ndc)-Ni-β** (c) and **sql-(1,3-bib)(ndc)-Ni-α′** (d); (e) guest water molecules in sql-(1,3-bib)(ndc)-Ni-β and sql-(1,3-bib)(ndc)-Ni-α′. Hydrogen atoms are omitted for clarity.

phase with reduced porosity, **sql-(1,3-bib)(ndc)-Ni-β** (Fig. 2c). Both the unit cell volume and the interlayer distance had contracted to 5857.2 Å^3 and 7.047 Å, respectively, while the PXRD pattern revealed peaks shifted to higher 2θ values (Fig. S8, S17 and Table S2, ESI†). A TG trace indicated that this phase had reduced porosity, a guest-accessible space of 7.7% along the cavities and channels filled with H_2O molecules adsorbed from laboratory atmosphere (Fig. S10 and S21, ESI†). A hydrogen-bonded H_2O molecule was located within 2.777 Å of the two adjacent aqua ligands (Fig. S12, ESI†), along with an additional H_2O molecule in the interlayer space. SCXRD of the **β** phase conducted in a capillary sealed under dynamic vacuum indicated that the hydrogen-bonded H_2O molecule remained even under activation conditions (Fig. S12 and S22, ESI†). Further, VT-PXRD measurements revealed that heating **sql-(1,3-bib)(ndc)-Ni-β** under vacuum did not induce a phase change until eventual decomposition, consistent with structural rigidity despite removal of guest water molecules (Fig. S23, ESI†).

The response of **sql-(1,3-bib)(ndc)-Ni-β** to water vapour prompted us to investigate its behaviour towards water. When **sql-(1,3-bib)(ndc)-Ni-β** was immersed in water, a new phase, **sql-(1,3-bib)(ndc)-Ni-α′**, was obtained (Fig. 2d), with a PXRD pattern resembling that of **sql-(1,3-bib)(ndc)-Ni-α** (Fig. S17, ESI†). **sql-(1,3-bib)(ndc)-Ni-α′** had crystallised with a unit cell volume of 6296.4 Å^3 and its interlayer distances were found to be 7.608 Å (compared to 6279.8 Å^3 and 7.644 Å for **α**). Even though **α′** has similar guest-accessible space to **α**, its voids are filled with water, as suggested by its TG profile (Fig. S24, ESI†). SCXRD analysis afforded the location of the hydrate molecules, including that between two Ni centres (O···O = 2.777 Å, Fig. S12, ESI†). Hydrate molecules were located in seven other positions with partial occupancies, amounting to four H_2O molecules per Ni (Fig. 2e). FTIR spectroscopy further indicated that **α′** can adsorb more water than **β**, transforming to a phase with the water content of **β** when left in air for 5 minutes (Fig. S14, ESI†).

Analysis of the crystal structures of **α**, **β**, **γ** and **α′** provided a plausible mechanism for the flexibility induced by water vapour. The flexible nature of 1,3-bib facilitated twisting of the imidazole rings with respect to the central phenyl ring, while the carboxylate carbon atoms in ndc enabled elongation/shrinkage of the linker (Fig. S25 and S26, ESI†). Consequently, intra-network adjacent Ni···Ni distances changed from 11.267 Å in **α** to 11.403, 10.980 and 11.290 Å in **β**, **γ** and **α′**, respectively. With respect to water vapour sorption, a hydrate molecule in **β** (O1B) interacting with an uncoordinated oxygen atom from the ndc ligand hydrogen bonds with other water molecules at high humidity, resulting in **α′** (Fig. S27 and Tables S4, S5, ESI†). Furthermore, while the hydrogen bonded hydrate molecule in **α**, **γ** and **α′** is held in place by H···O interactions within the same net, one of these interactions in **β** is replaced by an H···O bond with an adjacent net. Indeed, this acts as a driving force for converting **α** to **β**, bringing the individual nets closer together (Fig. S12, ESI†).

Dynamic vapour sorption (DVS) experiments were conducted on **sql-(1,3-bib)(ndc)-Ni-β**, which exhibited a variant of an S-shaped (in particular, a type F-II[35]) isotherm when exposed to water vapour (Fig. 3a), which is consistent with flexibility. PXRD patterns at various levels of relative humidity (RH; 0, 30 and 100%; Fig. 3b and Fig. S28, ESI†) indicated that it underwent reversible transformation induced by water vapour between the **β** (0% RH) and **α′** (100% RH) phases. The maximum uptake was observed to be 101.3 cm^3 g^{-1}, in agreement with the SCXRD data for **α′** (calculated 107.4 cm^3 g^{-1}, Table S6, ESI†).

Gas sorption studies on **sql-(1,3-bib)(ndc)-Ni-β** at cryogenic temperatures for CO_2 (195 K) and N_2 (77 K) revealed adsorption of CO_2 but not N_2, an indication that it could be a CO_2/N_2 sieve (Fig. S29, ESI†). Specifically, **β** showed a type F-II isotherm profile[35] towards CO_2 with a saturation uptake of 74.7 cm^3 g^{-1} at 1 bar, resembling the shape of the water isotherm and indicating flexibility. Isotherms consistent with flexibility were also observed for C2 gases (C_2H_2, C_2H_4 and C_2H_6) at 273 and 298 K (Fig. S30 and S31, ESI†). In contrast, **β** showed no evidence flexibility towards CO_2 at 273 and 298 K, while registering negligible uptake for CH_4 (at both temperatures) and N_2 (at 298 K) (Fig. 3c and Fig. S32, ESI†). The recorded uptakes of CO_2 at 1 bar were 25.5 and 16.8 cm^3 g^{-1} at 273 and 298 K, respectively. Ideal adsorbed solution theory (IAST) afforded selectivities of 36.6 for CO_2/N_2 (15 : 85) and 16.0 for CO_2/CH_4 (50 : 50), at 1 bar (Table S7 and Fig. S33, ESI†). The pressure-dependent selectivity values obtained are characteristic of sieving and show the limited applicability of IAST to such an adsorbent, in which equivalent adsorption sites are not

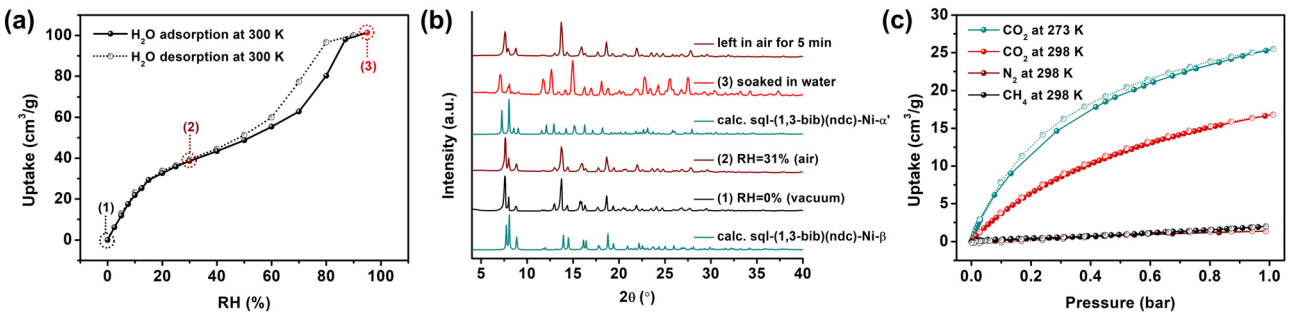

Fig. 3 (a) Water vapour sorption isotherm recorded on **sql-(1,3-bib)(ndc)-Ni-β** at 300 K; (b) calculated (calc.) and experimental PXRD patterns collected at various relative humidity (RH) values and room temperature; (c) gas sorption isotherms for CO_2 (at 273 and 298 K), N_2 and CH_4 (at 298 K).

available to competing adsorbate species.[36] *In situ* PXRD study of CO_2-loaded **sql-(1,3-bib)(ndc)-Ni-β** collected at 298 K revealed that exposure to CO_2 up to 1 bar did not trigger a phase change (Fig. S34, ESI†). Conversely, the PXRD patterns collected at 0.5 and 1.0 bar are consistent with micropore adsorption in the narrow-pore **β** phase.

In summary, we report the prototypal member of a new type of 2D coordination network, **sql-(1,3-bib)(ndc)-Ni**, and detail its structural flexibility towards water vapour and organic guests (DMA and methanol). SCXRD studies verified structural transformations from the as-synthesized **α** phase, initially to a more porous phase, **γ**, and eventually to a less porous phase, **β**. Water vapour sorption studies revealed that humidity (>50% RH) induced transformation of **β** to a phase resembling the as-synthesised phase, **α′**. SCXRD data enabled us to determine the location of the adsorbed water molecules, providing insight into the flexibility of **sql-(1,3-bib)(ndc)-Ni**. Moreover, gas sorption experiments indicated that **β** behaved as a sieve for CO_2 over N_2 and CH_4. Given the large number of 2D networks archived in the CSD, these findings suggest that other CNs with aqua ligands offer potential as reversible, flexible desiccants.

This work was financially supported by the Irish Research Council (IRCLA/2019/167) and Science Foundation Ireland (16/IA/4624). S. M. acknowledges an SFI-IRC Pathway award (21/PATH-S/9454) from the Science Foundation Ireland.

Conflicts of interest

There are no conflicts to declare.

Notes and references

1 B. Moulton and M. J. Zaworotko, *Chem. Rev.*, 2001, **101**, 1629–1658.
2 G. Desiraju, *IUCrJ*, 2017, **4**, 710–711.
3 B. F. Hoskins and R. Robson, *J. Am. Chem. Soc.*, 1990, **112**, 1546–1554.
4 Z. Zhang, S. B. Peh, C. Kang, K. Chai and D. Zhao, *Energy Chem.*, 2021, **3**, 100057.
5 R.-B. Lin, S. Xiang, H. Xing, W. Zhou and B. Chen, *Coord. Chem. Rev.*, 2019, **378**, 87–103.
6 S. Mukherjee, D. Sensharma, K.-J. Chen and M. J. Zaworotko, *Chem. Commun.*, 2020, **56**, 10419–10441.
7 K. Sumida, D. L. Rogow, J. A. Mason, T. M. McDonald, E. D. Bloch, Z. R. Herm, T.-H. Bae and J. R. Long, *Chem. Rev.*, 2012, **112**, 724–781.
8 C. A. Trickett, A. Helal, B. A. Al-Maythalony, Z. H. Yamani, K. E. Cordova and O. M. Yaghi, *Nat. Rev. Mater.*, 2017, **2**, 17045.
9 P. Nugent, Y. Belmabkhout, S. D. Burd, A. J. Cairns, R. Luebke, K. Forrest, T. Pham, S. Ma, B. Space, L. Wojtas, M. Eddaoudi and M. J. Zaworotko, *Nature*, 2013, **495**, 80–84.
10 S. Mukherjee, N. Sikdar, D. O'Nolan, D. M. Franz, V. Gascón, A. Kumar, N. Kumar, H. S. Scott, D. G. Madden, P. E. Kruger, B. Space and M. J. Zaworotko, *Sci. Adv.*, 2019, **5**, eaax9171.
11 H. Kim, S. Yang, S. R. Rao, S. Narayanan, E. A. Kapustin, H. Furukawa, A. S. Umans, O. M. Yaghi and E. N. Wang, *Science*, 2017, **356**, 430–434.
12 A. Kondo, H. Noguchi, S. Ohnishi, H. Kajiro, A. Tohdoh, Y. Hattori, W.-C. Xu, H. Tanaka, H. Kanoh and K. Kaneko, *Nano Lett.*, 2006, **6**, 2581–2584.
13 M. Fujita, Y. J. Kwon, S. Washizu and K. Ogura, *J. Am. Chem. Soc.*, 1994, **116**, 1151–1152.
14 H. Kajiro, A. Kondo, K. Kaneko and H. Kanoh, *Int. J. Mol. Sci.*, 2010, **11**, 3803–3845.
15 J. Shen, X. He, T. Ke, R. Krishna, J. M. van Baten, R. Chen, Z. Bao, H. Xing, M. Dinca, Z. Zhang, Q. Yang and Q. Ren, *Nat. Commun.*, 2020, **11**, 6259.
16 M. Shivanna, K.-i Otake, B.-Q. Song, L. M. van Wyk, Q.-Y. Yang, N. Kumar, W. K. Feldmann, T. Pham, S. Suepaul, B. Space, L. J. Barbour, S. Kitagawa and M. J. Zaworotko, *Angew. Chem., Int. Ed.*, 2021, **60**, 20383–20390.
17 J. Wang, Y. Zhang, Y. Su, X. Liu, P. Zhang, R.-B. Lin, S. Chen, Q. Deng, Z. Zeng, S. Deng and B. Chen, *Nat. Commun.*, 2022, **13**, 200.
18 V. I. Nikolayenko, D. C. Castell, D. Sensharma, M. Shivanna, L. K. A. Forrest, C. J. Solanilla-Salinas, K.-I. Otake, S. Kitagawa, L. J. Barbour, B. Space and M. J. Zaworotko, *Nat. Chem.*, 2023, **15**, 542–549.
19 P. Müller, F. M. Wisser, V. Bon, R. Grünker, I. Senkovska and S. Kaskel, *Chem. Mater.*, 2015, **27**, 2460–2467.
20 L. Schlechte, V. Bon, R. Grünker, N. Klein, I. Senkovska and S. Kaskel, *Polyhedron*, 2012, **44**, 179–186.
21 K. Koupepidou, V. I. Nikolayenko, D. Sensharma, A. A. Bezrukov, M. Shivanna, D. C. Castell, S.-Q. Wang, N. Kumar, K.-I. Otake, S. Kitagawa and M. J. Zaworotko, *Chem. Mater.*, 2023, **35**, 3660–3670.
22 K. Koupepidou, V. I. Nikolayenko, D. Sensharma, A. A. Bezrukov, M. Vandichel, S. J. Nikkhah, D. C. Castell, K. A. Oyekan, N. Kumar, A. Subanbekova, W. G. Vandenberghe, K. Tan, L. J. Barbour and M. J. Zaworotko, *J. Am. Chem. Soc.*, 2023, **145**, 10197–10207.
23 B.-Q. Song, Q.-Y. Yang, S.-Q. Wang, M. Vandichel, A. Kumar, C. Crowley, N. Kumar, C.-H. Deng, V. GasconPerez, M. Lusi, H. Wu, W. Zhou and M. J. Zaworotko, *J. Am. Chem. Soc.*, 2020, **142**, 6896–6901.
24 V. A. Blatov, A. P. Shevchenko and D. M. Proserpio, *Cryst. Growth Des.*, 2014, **14**, 3576–3586.
25 I. J. Bruno, J. C. Cole, P. R. Edgington, M. Kessler, C. F. Macrae, P. McCabe, J. Pearson and R. Taylor, *Acta Crystallogr., Sect. B: Struct. Sci.*, 2002, **58**, 389–397.
26 A. A. Bezrukov, D. J. O'Hearn, V. Gascón-Pérez, S. Darwish, A. Kumar, S. Sanda, N. Kumar, K. Francis and M. J. Zaworotko, *Cell Rep. Phys. Sci.*, 2023, **4**, 101252.
27 A. Cadiau, J. S. Lee, D. Damasceno Borges, P. Fabry, T. Devic, M. T. Wharmby, C. Martineau, D. Foucher, F. Taulelle, C.-H. Jun, Y. K. Hwang, N. Stock, M. F. De Lange, F. Kapteijn, J. Gascon, G. Maurin, J.-S. Chang and C. Serre, *Adv. Mater.*, 2015, **27**, 4775–4780.
28 A. J. Rieth, S. Yang, E. N. Wang and M. Dincă, *ACS Cent. Sci.*, 2017, **3**, 668–672.
29 N. Hanikel, M. S. Prévot, F. Fathieh, E. A. Kapustin, H. Lyu, H. Wang, N. J. Diercks, T. G. Glover and O. M. Yaghi, *ACS Cent. Sci.*, 2019, **5**, 1699–1706.
30 T. Fukushima, S. Horike, Y. Inubushi, K. Nakagawa, Y. Kubota, M. Takata and S. Kitagawa, *Angew. Chem., Int. Ed.*, 2010, **49**, 4820–4824.
31 S. Krause, V. Bon, H. C. Du, R. E. Dunin-Borkowski, U. Stoeck, I. Senkovska and S. Kaskel, *Beilstein J. Nanotechnol.*, 2019, **10**, 1737–1744.
32 M. Magott, B. Gaweł, M. Sarewicz, M. Reczyński, K. Ogorzały, W. Makowski and D. Pinkowicz, *Chem. Sci.*, 2021, **12**, 9176–9188.
33 A. Subanbekova, V. I. Nikolayenko, A. A. Bezrukov, D. Sensharma, N. Kumar, D. J. O'Hearn, V. Bon, S.-Q. Wang, K. Koupepidou, S. Darwish, S. Kaskel and M. J. Zaworotko, *J. Mater. Chem. A*, 2023, **11**, 9691–9699.
34 X. Li, D. Sensharma, V. I. Nikolayenko, S. Darwish, A. A. Bezrukov, N. Kumar, W. Liu, X.-J. Kong, Z. Zhang and M. J. Zaworotko, *Chem. Mater.*, 2023, **35**, 783–791.
35 Q.-Y. Yang, P. Lama, S. Sen, M. Lusi, K.-J. Chen, W.-Y. Gao, M. Shivanna, T. Pham, N. Hosono, S. Kusaka, J. J. Perry IV, S. Ma, B. Space, L. J. Barbour, S. Kitagawa and M. J. Zaworotko, *Angew. Chem., Int. Ed.*, 2018, **57**, 5684–5689.
36 A. L. Myers and J. M. Prausnitz, *AlChE J.*, 1965, **11**, 121–127.

